SAND2016-3676C

Recent developments in interband cascade infrared photodetectors

Hossein Lotfi*, Lu Li, Lin Lei, Hao Ye, SM Shazzad Rassel, Yuchao Jiang, Rui Q. Yang*
School of Electrical and Computer Engineering, University of Oklahoma, Norman, OK, USA 73019
John F. Klem
Sandia National Laboratories, Albuquerque, NM, USA, 87185
Tetsuya D. Mishima, Michael B. Santos, Matthew B. Johnson
Department of Physics and Astronomy, University of Oklahoma, Norman, OK, USA, 73019
James A. Gupta
National Research Council of Canada, Ottawa, ON, Canada, K1A 0R6

ABSTRACT

We investigate high-temperature and high-frequency operation of interband cascade infrared photodetectors (ICIPs)-two critical properties. Short-wavelength ICIPs with a cutoff wavelength of 2.9 μm had Johnson-noise limited detectivity of 5.8×10^{9} cmHz$^{1/2}$/W at 300 K, comparable to the commercial $Hg_{1-x}Cd_xTe$ photodetectors of similar wavelengths. A simple but effective method to estimate the minority carrier diffusion length in short-wavelength ICIPs is introduced. Using this approach, the diffusion length was estimated to be significantly shorter than 1 μm at high temperatures, indicating the importance of a multiple-stage photodetector (e.g., ICIPs) at high temperatures. Recent investigations on the high-frequency operation of mid-wavelength ICIPs (λ_c=4.3 μm) are discussed. These photodetectors had 3-dB bandwidths up to 1.3 GHz with detectivities exceeding 1×10^{9} cmHz$^{1/2}$/W at room temperature. These results validate the ability of ICIPs to achieve high bandwidths with large sensitivity and demonstrate the great potential for applications such as: heterodyne detection, and free-space optical communication.

Keywords: III-V semiconductors, diffusion length, high-speed photodetectors, high-temperature operation, interband cascade structures, mid-wavelength infrared, short wavelength infrared, type-II superlattice.

1. INTRODUCTION

Since the early efforts on the ternary $Hg_{1-x}Cd_xTe$ alloy in 1959[1], this material system has remained the main player in infrared detection for different spectral bands. Photodetectors based on this material system are well developed, to the degree that their performance metrics are established as the benchmark[2] for emerging or competing technologies. However, $Hg_{1-x}Cd_xTe$ has certain drawbacks including: difficulties in growth, expensive and irregular substrates, and material nonuniformity. Such difficulties have stimulated decades of research for alternative material systems. Among different candidates, type-II superlattice (SL) photodetectors have shown promise to outperform their $Hg_{1-x}Cd_xTe$ based counterparts[3,4]. Nevertheless, type-II SLs have their own shortcomings, including: short carrier lifetime and limited diffusion length. These issues can be overcome utilizing a multiple-stage photodetector with multiple short absorbers used throughout the structure.

ICIPs utilize the unique features of the 6.1 Å family of semiconductors to construct multiple-stage interband photovoltaic detectors. Each stage in an ICIP is composed of three regions: electron barrier, absorber, and hole barrier. Absorbers in ICIPs can be made of SL[5,6] or bulk material[7], provided that the required band alignments are realized in different regions. Absorber thickness in each individual stage is shorter than the diffusion length of minority carriers. As such, ICIPs are able to collect most of the photogenerated carriers at high temperatures. Depending on the requirements for the device sensitivity and frequency response, the absorber thickness and the number of stages are adjusted in ICIPs. Owing to these design flexibilities, ICIPs are able to achieve high speed with large detectivity. Furthermore, ICIP's multiple-stage architecture and thin absorbers remove some of the stringent requirements on the material quality. A recent report on mid-wavelength ICIPs grown on GaAs substrates[8] shows that the performance of ICIPs is almost insensitive to the material quality.

*Email: hossein.lotfi@ou.edu; Rui.q.Yang@ou.edu; Phone: +1 (405) 325-7361; Fax: +1 (405) 325-7066; http://qdl.ou.edu

2. SHORT-WAVELENGTH ICIPS

2.1 Device structure

While ICIPs working in mid-wavelength IR (MWIR) to very-long-wavelength IR (VLWIR) spectral bands have been reported in the literatures[5,9,10], there has been no report on SWIR ICIPs until our recent work[11]. Such a short-wavelength ICIP can be a standalone detector or can be integrated with different band ICIPs to realize multi-color ICIPs. Multicolor ICIPs can be readily implemented using regular- and reverse-designed ICIPs. In a regular designed ICIP, photo-generated electrons travel in the same direction as the incident photons (see Figure 1) and most of the photo-generated electrons are away from the collecting layer (*i.e.*, hole barriers). The photo-generated electrons travel distance is significantly reduced in a reversed structure. In a reverse-designed ICIP, photogenerated electrons travel in opposite direction of incident photons and most of them are closer to the collection point(s). If the diffusion length falls shorter than the absorber thickness, the reverse design configuration will have higher collection efficiency for electrons compared to the regular configuration. Moreover, the reverse configuration should result in faster ICIPs because the photogenerated electrons travel a shorter distance before collection.

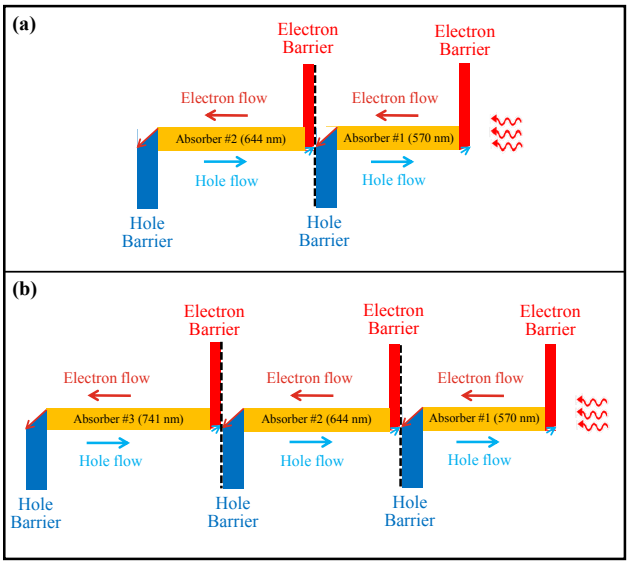

Figure 1: Schematic drawings of the regular-configuration SWIR ICIPs: (a) two-stage and (b) three-stage ICIPs. The photo-generated electrons and incident photons travel in the same direction in regular-configuration ICIPs.

Two regular-configuration SWIR ICIPs, one with two stages and one with three stages, were designed and grown by molecular beam epitaxy (MBE) on unintentionally doped GaSb substrates. Each period of the SL absorber was composed of InAs (20 Å)/ GaSb (15 Å)/ $Al_{0.2}In_{0.8}Sb$ (7 Å)/ and GaSb (15 Å) layers, in which GaSb layers were p-type doped. Electron barriers were made of three GaSb/AlSb quantum wells (QWs) and the hole barriers consisted of seven digitally graded InAs/AlSb QWs. The role of electron and hole barriers is to facilitate the separation and unidirectional flow of photo-generated electrons and holes in opposite directions. As shown in Figure 1, the two- and three-stage ICIPs had absorber thicknesses of 570 nm and 644 nm in the first and second stages, respectively. Absorbers were designed thicker in optically deeper stages to realize photocurrent matching between different stages. The third stage in the three-stage ICIP was 741-nm thick. All the other design and growth parameters such as the electron and hole barriers and the doping levels were kept the same in the ICIPs. Further details on the device band structure, processing and fabrication are provided elsewhere[11].

2.2 Electrical characteristics

2.2.1 Dark current

The high temperature (T=280-340 K) dark J-V curves for the two- and three-stage SWIR ICIPs are shown in Figure 2. Dark current densities were lower in three-stage ICIPs at all temperatures. For example, the room temperature (T=300 K) dark current density of a representative 1.0×1.0 mm^2 two- and three-stage ICIP at -50 mV was 8.4 and 5.5 mA/cm^2, respectively. Generally, dark current densities were larger in smaller-sized ICIPs for both detector arrays, which is attributed to surface leakage current. A detailed

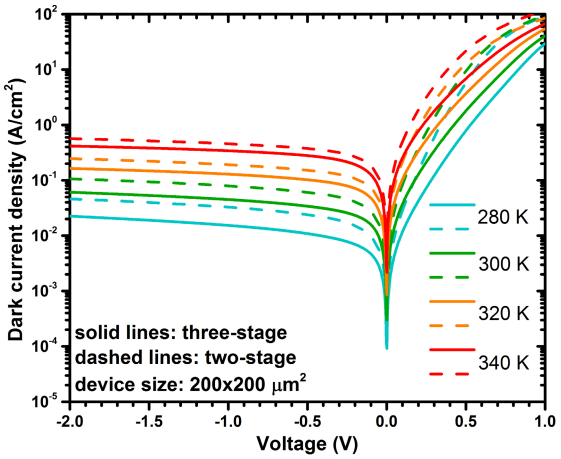

Figure 2: Dark current density for representative two- and three- stage SWIR ICIPs for T=280-340 K.

discussion on the origins of their size-dependent dark currents is provided in Ref 11.

2.2.2 Diffusion length in SWIR ICIPs

At high temperatures, most of the material parameters (*e.g.*, diffusion length and carrier lifetime) are unknown for the type-II SL material system. Often, diffusion length is inferred from the measurements of other parameters such as carrier mobility and lifetime. These techniques require very precise setups and complicated optics[12-14]. An easier approach to extract the material parameters is to fit the dark current *I-V* curves to the detailed mathematical equations used for carrier transport in photodetectors. In these models, a large number of fitting parameters[15] could result in uncertainties in the extracted parameters.

Here we propose a very simple, yet effective, technique to extract the diffusion length and its temperature dependency in interband cascade photodetectors. Although we have applied this technique to ICIPs at high temperatures, it can be used with any type of semiconductor devices and at any temperature, provided that the device dark current is dominated by diffusion. This technique requires, at least, two photodetectors with similar designs but different absorber thicknesses and/or number of stages. Having a larger set of similar detectors results in a more accurate determination of diffusion length. While there is some uncertainty in the reported numbers, as further described later, we have presented this technique for the benefit of the detector community. Further modifications and more results will be presented elsewhere.

The device zero-bias resistance and area product (R_0A) in a diffusion-limited ICIP, with electrons as the minority carriers, is described by[16]:

$$R_0A = \frac{k_BT\sum_m \frac{1}{\tanh\left(d_m/L_e\right)}}{q^2 g_{th} L_e}, \tag{1}$$

where k_B, T, d_m, L_e, g_{th} and q are Boltzmann constant, absolute temperature, absorber thickness in the m^{th} stage, electron diffusion length, thermal generation rate and electric charge, respectively. Note that this equation is also applicable to single-stage photodetectors. Once the diffusion-limited behavior of the device dark current is assured (this can be examined by the device activation energy or observance of a flat region in the device dark *I-V*), the above equation can be used to extract the device diffusion length. In this equation, there are two unknowns, diffusion length and thermal generation rate. By using the R_0A ratio between two photodetectors with different absorber thicknesses or number of stages, we can remove the thermal generation rate. For example, the R_0A ratio for the two SWIR ICIPs reported in this work was:

$$\frac{(R_0A)_{three-stage}}{(R_0A)_{two-stage}} = \frac{\frac{1}{\tanh\left(d_1/L_e\right)} + \frac{1}{\tanh\left(d_2/L_e\right)} + \frac{1}{\tanh\left(d_3/L_e\right)}}{\frac{1}{\tanh\left(d_1/L_e\right)} + \frac{1}{\tanh\left(d_2/L_e\right)}}, \tag{2}$$

where, d_1 and d_2 are the absorber thickness in the first and second stage of the two ICIPs and d_3 denotes the absorber thickness in the third stage of the three-stage ICIP. Because the R_0A ratio in Equation 2 is known from the measurements, the device diffusion length (L_e), as the only unknown, can be readily found for each temperature.

There are four requirements related to this approach:

(1) Surface leakage currents are neglected in Equation 2. These currents are often present in type-II SL detectors, thus, $(R_0A)_{bulk}$, which can be extracted from the plot of different sized detectors R_0A, can be used for more accurate determination of the diffusion length.

(2) The device's series resistance and the parasitic resistances from the measurement setup should be excluded from the device measured resistance. In narrow bandgap photodetectors, these parasitic resistances are in the same order of magnitude of the device resistance for certain device sizes at high temperatures and could result in significant uncertainty in the diffusion length estimation.

(3) The above ratio should be obtained for detectors with similar material and processing quality. To ensure this assumption, the two SWIR ICIPs were grown by the same MBE system and in two consecutive growth runs with similar growth conditions.

(4) The carriers' transport should be controlled by minority carriers. Depending on the device bandgap, temperature, and the absorber doping level, ambipolar effects *(i.e.* both electrons and holes) could start to control the transport dynamics.

Because the surface leakage currents are present in the SWIR ICIPs, the $(R_0A)_{bulk}$ extracted from the size-dependent plot of different-sized ICIPs was used for the R_0A ratios. Figure 3 shows the theoretical R_0A ratio for the two- and three-stage ICIPs versus diffusion length. The single points on this curve represent the calculated ratios of the measured R_0A values for T=300-340 K. The minority carrier diffusion length was estimated to be 450 nm at 300 K. The extracted diffusion lengths at different temperatures along with the R_0A ratios are summarized in Table 1. Diffusion lengths were well below 1 μm at high temperatures. Typically, type-II SL detectors have absorber thickness of 1 to 3 μm. While thick absorbers are required for sufficient photon absorption, short diffusion lengths limit the device quantum efficiency and only photogenerated carriers generated within a diffusion length of the collection point(s) will contribute to the device quantum efficiency and the rest of carries are wasted.

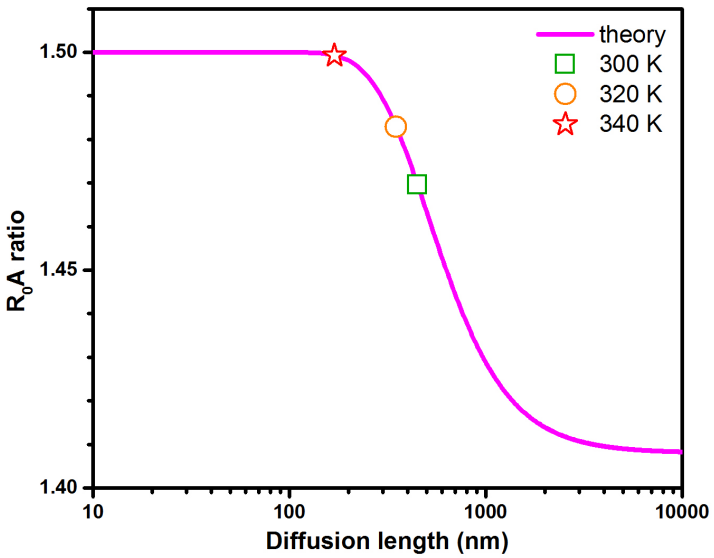

Figure 3: The theoretical curve and the measured R_0A ratios (single points on the curve) for T=300- 340 K. The device dark current was dominated by the diffusion process in this temperature range.

Table 1 Summary of the measured and extracted parameters for two- and three-stage SWIR ICIPs at room temperature and above.

Temperature (K)	$(R_0A)_{bulk}$ ($\Omega.cm^2$)		$\frac{(R_0A)_{Three-stage}}{(R_0A)_{Two-stage}}$	Diffusion length (nm)
	Two-stage	Three-stage		
300	5.446	8.006	1.470	450
320	1.738	2.578	1.483	350
340	0.612	0.918	1.500	≤170

2.3 Optical characteristics

The responsivity of the two SWIR ICIPs was measured using an FTIR spectrometer and a calibrated 800 K blackbody source, placed 30 cm away from the detectors. Figures 4 (a) & (b) show the zero-bias response for representative two- and three-stage ICIPs for T=280-340 K. The zero-bias responsivity was nearly constant for both ICIPs in this temperature range, indicating the ability of ICIPs to efficiently collect the photogenerated carriers at high temperatures. At λ=2.1 μm, the responsivity in the three-stage ICIPs was 16% lower than in the two-stage ICIPs. This is probably due to the imperfect photocurrent matching between different stages. Normalized Johnson-noise limited detectivity (at λ=2.1 μm) was 5.1×10^9 and 5.8×10^9 $cmHz^{1/2}/W$ for two- and three-stage ICIPs at 300 K. As shown in Figure 4 (c), the normalized detectivity was larger in three-stage ICIPs at all temperatures. With improved photocurrent matching, larger detectivities are expected for the three-stage ICIPs.

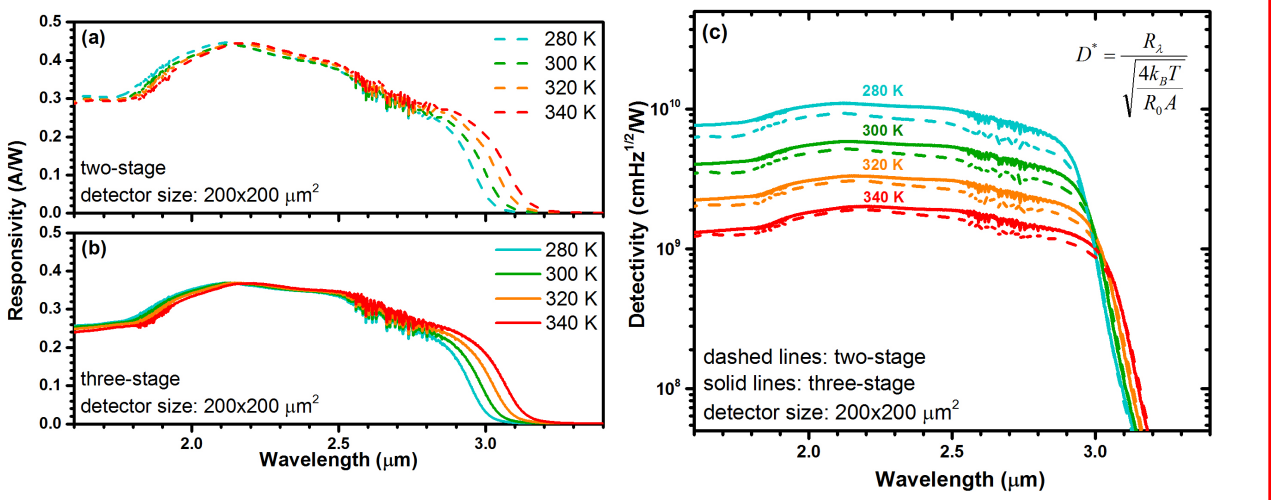

Figure 4: Optical characteristics of the SWIR ICIPs: (a) Zero-bias responsivity for the two-stage ICIPs, (b) Zero-bias responsivity for three-stage ICIPs, and (c) Johnson-noise limited detectivity for two- and three-stage devices.

3. HIGH-FREQUENCY OPERATION OF INTERBAND CASCADE DEVICES

3.1 Background

While many features of ICIPs (*e.g.*, high-temperature operation with high detectivities, large device resistance, and low noise have been investigated[5,6,9,10,17]) the high-speed operation of ICIPs has not been studied until this work. The common approach to achieve high speed in conventional photodetectors is to decrease the absorber thickness. Although thin absorbers decrease the carriers' transit time, the reduced quantum efficiency (QE) has a negative influence on the device sensitivity. For this reason, the product of the device sensitivity and bandwidth remains constant in single-stage photodetectors. In contrast to conventional single-stage photodetectors, where the high-frequency response costs on the device sensitivity, ICIPs can simultaneously achieve high speed and large sensitivity. In thin-absorber ICIPs, the photogenerated carriers travel very short distances (in the nm range), which results in short transit times. And the multiple-stage structure of ICIPs secures large absorption efficiency and reduces the device noise.

In order to study the high-speed performance of ICIPs at room temperature, mid-wavelength ICIPs (λ_c=4.3 μm) with a different number of stages and absorber thicknesses were designed and grown by MBE. Figure 5 (a) shows the zero-bias responsivity and Johnson-noise limited detectivity (D^*) spectra of a three-stage reverse-configuration ICIP. The absorber thicknesses were 312, 344.5 and 383.5 nm in the first, second and the third stages, respectively. The device responsivity was 0.25 A/W and its D^* exceeded 10^9 cmHz$^{1/2}$/W at 3 μm. Because of the thin absorbers, we can reasonably assume that almost all of the photo-generated carriers are collected. As such, the absorption coefficient is estimated to be larger than 5,400 cm^{-1}. This number is significantly larger than the expected values for type-II SL absorbers. To further investigate the large responsivities observed in these ICIPs, a one-stage ICIP with absorber thickness of 1,040 nm was grown to directly measure the absorption coefficient of the SL. The absorption coefficient spectrum obtained from the transmission measurement is shown in Figure 5 (b). The measured absorption coefficient was ~3,300 cm^{-1} at 3 μm, which is significantly smaller than the number extracted from the response measurements. The large responsivities observed in these ICIPs are attributed to a possible gain mechanism in their structure. The short absorbers employed in these ICIPs could result in a gain mechanism similar to gain in photoconductors. If the carriers' transit time become shorter than their lifetime, it is possible to have gain in the device structure. Further investigations are needed to understand the source of gain in these ICIPs.

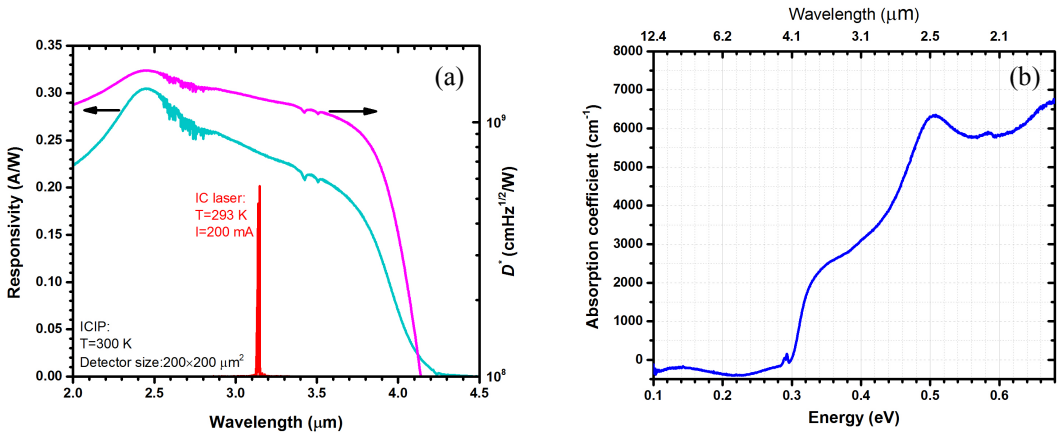

Figure 5: (a) The measured responsivity and normalized detectivity for the three-stage mid-wavelength ICIP. The emission spectrum for the IC laser used in the high-frequency modulation is also provided. (b) The absorption spectrum for the type-II SL measured at room temperature.

3.2 High-frequency modulation setup and characterization

In order to study the high-frequency characteristics of ICIPs, an optical setup consisted of a type-I interband cascade (IC) laser[18] and an ICIP was constructed, as shown in Figure 6. The IC laser was operated at T=293 K and was biased above the lasing threshold at 200 mA DC current. The RF signal was sweep-generated (200 kHz-1.2 GHz) by an analog signal generator. The laser output was then collimated and focused on the ICIP using a pair of germanium lenses.

The DC and AC output signals from the detector were then separated with a bias-tee and the RF signal was fed to a spectrum analyzer.

The measured frequency response includes the frequency response of the IC laser and the ICIP. Figure 7 shows the measured frequency response of three different-sized ICIPs from the three-stage MWIR wafer. Note that the same IC laser was used during the high-frequency characterizations. The system frequency bandwidth was lower for larger size ICIPs. This suggests the system performance was limited by parasitic elements. The MWIR high-frequency system had a 3-dB bandwidth of 850 MHz with a 20×20 μm² ICIP.

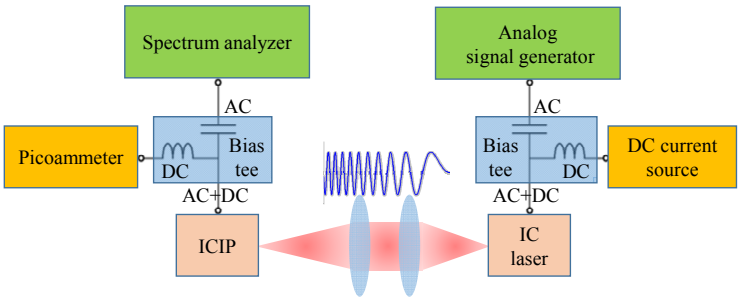

Figure 6: Schematic diagram for the high-frequency modulation setup used to characterize the high-frequency performance of MWIR ICIPs.

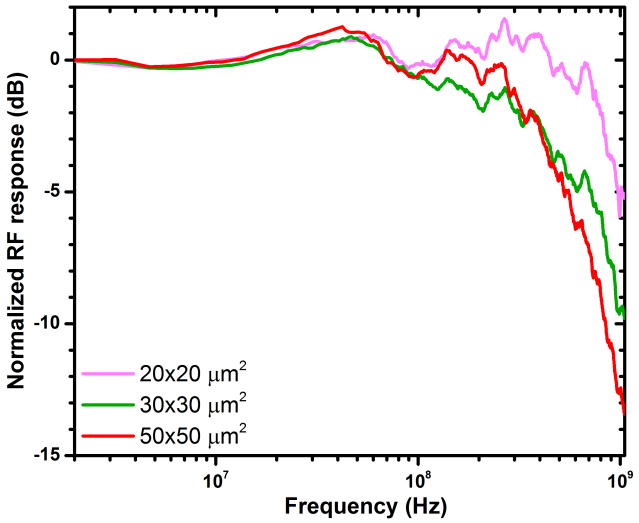

Figure 7: The measured frequency response for the MWIR interband cascade system with different-sized ICIPs.

In order to identify the 3-dB bandwidth of the IC laser and the ICIPs, a circuit model is introduced (see Figure 8). Most of the circuit parameters such as the device series resistance (R_s), bonding pad capacitance (C_{bp}), bonding wire inductance (L_{bw}) and its resistance (R_{bw}) were directly measured or calculated. The only unknown parameter in the circuit model was the ICIP capacitance (C_d). Device capacitance was set as a fitting parameter to satisfy the measured 3-dB bandwidth. The calculated 3-dB bandwidth for the IC laser was 760 MHz, which was mainly limited by the bonding pad capacitance. The measured system bandwidth was generally higher in smaller-sized ICIPs indicating that the system bandwidth was limited by parasitic capacitances and inductances. Bonding wires, wires and coaxial cables used in the setup and bonding pad capacitances were the main sources of parasitic elements. The extracted 3-dB bandwidth for a 20×20 μm^2 three-stage ICIP was 1.3 GHz at room temperature. Representative ICIPs from this wafer had Johnson-noise limited detectivities larger than 10^9 cmHz$^{1/2}$/W (Figure 5) at room temperature. These preliminary results demonstrate the ability of ICIPs to achieve high-speed performance with a large device sensitivity even at high temperatures.

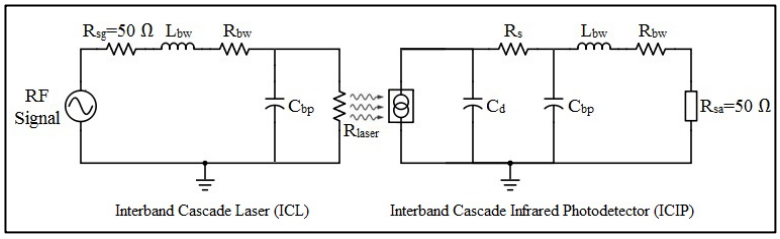

Figure 8: The equivalent circuit used to model the high-frequency interband cascade system. R_{sg} and R_{sa} are the output resistance of the signal generator and the input resistance of the spectrum analyzer, respectively.

3.3 Time-domain characterization

While the frequency domain measurements are an effective tool to examine the performance of a mid-IR link, the time domain measurements (*e.g.* eye diagrams) provide valuable information related to the signal integrity and the quality of the optical link. The time domain setup was very similar to our high-frequency domain setup (Figure 6). Instead of the analog signal generator, an arbitrary waveform generator (AWG) was used to generate pseudo-random bit sequences (PRBS). Each period of the PRBS had 16 random bits (zeros and ones). On the receiver end, a high-frequency oscilloscope was used to capture the received bits. The eye diagrams generated for three different ICIPs with different number of stages and absorber thicknesses are displayed in Figure 9. The absorber thickness was 1,040 nm in the one-stage ICIP, whereas the thickest absorbers were 383.5 and 591.5 nm in three- and eight-stage ICIPs, respectively. Note that the AWG was able to generate PRBS with bit rates up to 50 Mb/s. Based on the frequency domain measurements of the interband cascade system, clear and open eyes in significantly higher bit rates are expected. The generated eyes show limited rise and fall times in the one-stage ICIP at 48 Mb/s, while the other two ICIPs (three- and eight-stage ICIPs) with short absorbers and more stages did not exhibit any signal degradation up to this bit rate. Although all three ICIPs had similar detectivities (~10^9 cmHz$^{1/2}$/W) at room temperature, the one-stage ICIP had degraded performance compared to the other two ICIPs, showing that short absorbers and multiple stages are beneficial for high-speed applications.

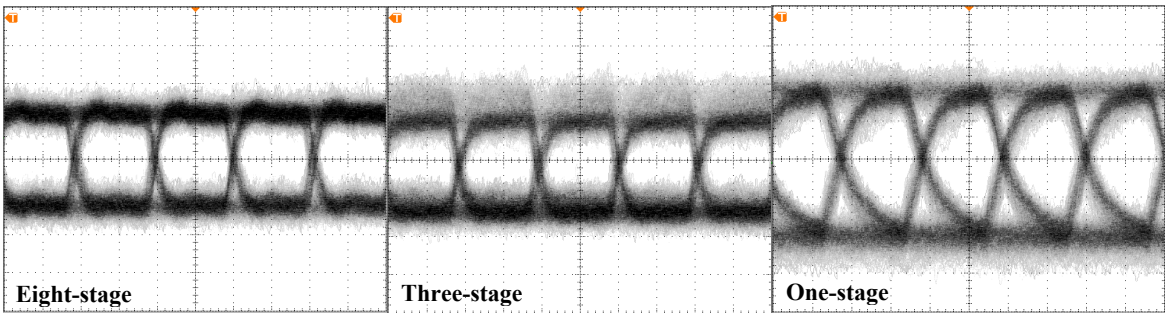

Figure 9: Eye diagrams for ICIPs with different number of stages and absorber thicknesses. Each horizontal division is 10 ns. Bit rate was 48 Mb/s.

4. SUMMARY AND CONCLUSION

We report recent progress in the development of high-temperature and high-frequency ICIPs. Three-stage SWIR ICIPs had larger detectivities than the two-stage counterparts, demonstrating the benefit of using more stages in these ICIPs.

These devices had Johnson-noise limited detectivities comparable to the-state-of-the-art $Hg_{1-x}Cd_xTe$ detectors for similar wavelengths. The extracted diffusion lengths at high temperatures were significantly shorter than the absorber thickness in a typical single-stage type-II SL IR photodetector. Therefore, multiple-stage photodetectors such as ICIPs are required at high temperatures.

Our high-frequency mid-wavelength interband cascade system (consisting of IC lasers and ICIPs) had a 3-dB bandwidth exceeding 800 MHz at room temperature. The high-speed and high-sensitivity characteristics of ICIPs along with high efficiency of IC lasers demonstrate the great promise of the interband cascade systems for applications such as heterodyne detection, free space optical communication and high-speed spectroscopy.

ACKNOWLEDGEMENT

This work was supported in part by AFOSR under Award FA9550-15-1- 0067. Sandia National Laboratories is a multi-program laboratory managed and operated by Sandia Corporation, a wholly owned subsidiary of LockheedMartin Corporation, for the U.S. Department of Energy's National Nuclear Security Administration under Contract DE-AC04-94AL85000.

REFERENCES

[1] Lawson, W. D., Nielsen, S., Putley, E. H., Young, A. S., "Preparation and properties of HgTe and mixed crystals of HgTe-CdTe," J. Phys. Chem. Solids **9**(3-4), 325–329 (1959).

[2] Tennant, W. E., Lee, D., Zandian, M., Piquette, E., Carmody, M., "MBE HgCdTe Technology: A Very General Solution to IR Detection, Described by 'Rule 07', a Very Convenient Heuristic," J. Electron. Mater. **37**(9), 1406–1410 (2008).

[3] Grein, C. H., Young, P. M., Ehrenreich, H., "Minority carrier lifetimes in ideal InGaSb/InAs superlattices," Appl. Phys. Lett. **61**(24), 2905 (1992).

[4] Smith, D. L., Mailhiot, C., "Proposal for strained type II superlattice infrared detectors," J. Appl. Phys. **62**(6), 2545–2548 (1987).

[5] Yang, R. Q., Tian, Z., Cai, Z., Klem, J. F., Johnson, M. B., Liu, H. C., "Interband-cascade infrared photodetectors with superlattice absorbers," J. Appl. Phys. **107**(5), 054514 (2010).

[6] Tian, Z., Hinkey, R. T., Yang, R. Q., Lubyshev, D., Qiu, Y., Fastenau, J. M., Liu, A. W. K., Johnson, M. B., "Interband cascade infrared photodetectors with enhanced electron barriers and p-type superlattice absorbers," J. Appl. Phys. **111**(2), 024510 (2012).

[7] Lei, L. et al, The University of Oklahoma and IQE, to be published.

[8] Tian, Z. B., Krishna, S., "Mid-infrared metamorphic interband cascade photodetectors on GaAs substrates," Appl. Phys. Lett. **107**(21), 211114 (2015).

[9] Lotfi, H., Li, L., Ye, H., Hinkey, R. T., Lei, L., Yang, R. Q., Keay, J. C., Mishima, T. D., Santos, M. B., Johnson, M. B., "Interband cascade infrared photodetectors with long and very-long cutoff wavelengths," Infrared Phys. Technol. **70**, 162–167 (2015).

[10] Lotfi, H., Lei, L., Li, L., Yang, R. Q., Keay, J. C., Johnson, M. B., Qiu, Y., Lubyshev, D., Fastenau, J. M., Liu, A. W. K., "High-temperature operation of interband cascade infrared photodetectors with cutoff wavelengths near 8 μ m," Opt. Eng. **54**(6), 063103 (2015).

[11] Lotfi, H., Li, L., Lei, L., Yang, R. Q., Klem, J. F., Johnson, M. B., "Short-wavelength interband cascade infrared photodetectors operating above room temperature," J. Appl. Phys. **119**, 023105 (2016).

[12] Connelly, B. C., Metcalfe, G. D., Shen, H., Wraback, M., "Direct minority carrier lifetime measurements and recombination mechanisms in long-wave infrared type II superlattices using time-resolved photoluminescence," Appl. Phys. Lett. **97**(25), 251117 (2010).

[13] Klein, B., Gautam, N., Plis, E., Schuler-Sandy, T., Rotter, T. J., Krishna, S., Connelly, B. C., Metcalfe, G. D., Shen, P., Wraback, M., "Carrier lifetime studies in midwave infrared type-II InAs/GaSb strained layer superlattice," J. Vac. Sci. Technol. B, **32**(2), 02C101 (2014).

[14] Höglund, L., Soibel, A., Ting, D. Z., Khoshakhlagh, A., Hill, C. J., Gunapala, S. D., "Minority carrier lifetime and photoluminescence studies of antimony-based superlattices," Proc. SPIE, M. Strojnik and G. Paez, Eds., 851106 (2013).

[15] Yang, Q. K., Fuchs, F., Schmitz, J., Pletschen, W., "Investigation of trap-assisted tunneling current in InAs/(GaIn)Sb superlattice long-wavelength photodiodes," Appl. Phys. Lett. **81**(25), 4757 (2002).

[16] Hinkey, R. T., Yang, R. Q., "Theory of multiple-stage interband photovoltaic devices and ultimate performance limit comparison of multiple-stage and single-stage interband infrared detectors," J. Appl. Phys. **114**(10), 104506 (2013).

[17] Gautam, N., Myers, S., Barve, a. V., Klein, B., Smith, E. P., Rhiger, D. R., Dawson, L. R., Krishna, S., "High operating temperature interband cascade midwave infrared detector based on type-II InAs/GaSb strained layer superlattice," Appl. Phys. Lett. **101**(2), 021106 (2012).

[18] Jiang, Y., Li, L., Yang, R. Q., Gupta, J. A., Aers, G. C., Dupont, E., Baribeau, J. M., Wu, X., Johnson, M. B., "Type-I interband cascade lasers near 3.2 μm," Appl. Phys. Lett. **106**(4), 041117 (2015).